Hydrophilic Nanotube Supported Graphene–Water Dispersible Carbon Superstructure with Excellent Conductivity

Vasilios Georgakilas, Athanasios Demeslis, Evangelos Ntararas, Antonios Kouloumpis, Konstantinos Dimos, Dimitrios Gournis, Mikuláš Kocman, Michal Otyepka, and Radek Zbořil**

In this work, it is shown that the hydrophilic functionalized multiwall carbon nanotubes (MWCNs) can stabilize a large amount of pristine graphene nanosheets in pure water without the assistance of surfactants, ionic liquids, or hydrophilic polymers. Role of stabilizer is conveyed by highly hydrophilic carbon nanotubes, functionalized by dihydroxy phenyl groups, affording a stable dispersion at concentrations as high as 15 mg mL^{-1}. Such multidimensional (2D/1D) graphene/MWCN hybrid is found to be dispersible also in other polar organic solvents such as ethanol, isopropanol, *N*,*N*-dimethylformamide, ethylene glycol, and their mixtures. High-resolution transmission microscopy and atomic force microscopy (AFM) including a liquid mode AFM manifest several types of interaction including trapping of multiwalled carbon nanotubes between the graphene sheets or the modification of graphene edges. Molecular dynamic simulations show that formation of an assembly is kinetically controlled. Importantly, the hybrid can be deposited on the paper by drop casting or dispersed in water-soluble polymers resulting in record values of electrical conductivity (sheet resistance up to $R_s \approx 25\ \Omega\ sq^{-1}$ for free hybrid material and $R_s \approx 1300\ \Omega\ sq^{-1}$ for a polyvinilalcohol/hybrid composite film). Thus, these novel water dispersible carbon superstructures reveal a high application potential as conductive inks for inkjet printing or as highly conductive polymers.

1. Introduction

Graphene is one of the most promising carbon nanomaterials known, attracting tremendous interest due to its unique electronic, mechanical, and optical properties.[1] As the thinnest 2D nanostructure ever isolated, it offers great potential for various nanotechnology applications. Natural graphite is a perfect clean abundant source of graphene. However, the isolation of graphene from graphite using organic solvents is not straightforward due to the strong van der Walls interactions holding the graphene sheets together. Furthermore, the strongly hydrophobic pristine graphene sheets are often almost nondispersible in water in the absence of surfactants.

Since the first isolation of graphene by the micromechanical exfoliation of graphite,[2] several procedures have been developed exploiting graphite as the starting material. The most widely used method to date, albeit with several variations, is based on the reduction of graphene oxide (GO) produced from graphite using strong oxidizing agents. Although such reduction procedures have been successfully applied, the final graphitic nanostructures, usually called partly reduced graphene oxide (*r*GO), are of low quality, especially, with regard to the electrical conductivity or mechanical properties.[3] On the other hand, pure and high quality pristine graphene nanosheets have been isolated from graphite by liquid-phase exfoliation in various solvents, such as *N*-methyl-2-pyrrolidone (NMP),[4] ortho-dichlorobenzene (o-DCB),[5] perfluorinated aromatic solvents,[6] and dimethylformamide (DMF).[7,8] The main disadvantage of these procedures involves a frequent production of dilute graphene dispersions (0.1–1 mg mL^{-1}, with a few exceptions), which are not effective mainly due to the high cost, toxicity, and environmental impact of the organic solvents required. Similar disadvantages have been demonstrated when surfactants are employed to promote the dispersion and stabilization of graphene in organic solvents.[9]

The dispersion of pristine graphene in water poses a considerable challenge owing to the material strong hydrophobic character of the material. Water dispersions have remarkable advantages over those obtained in organic solvents, such as low cost, absence of solvent toxicity, capacity for green chemistry,

Prof. V. Georgakilas, A. Demeslis, Dr. E. Ntararas
Materials Science Department
University of Patras
26504 Rio, Greece
E-mail: viegeorgaki@upatras.gr
A. Kouloumpis, Dr. K. Dimos, Prof. D. Gournis
Department of Materials Science and Engineering
University of Ioannina
45110 Ioannina, Greece
Dr. M. Kocman, Prof. M. Otyepka, Prof. R. Zbořil
Regional Centre of Advanced Technologies and Materials
Department of Physical Chemistry
Faculty of Science
Palacky University in Olomouc
17. listopadu 1192/12, 771 46, Olomouc, Czech Republic
E-mail: radek.zboril@upol.cz

DOI: 10.1002/adfm.201403801

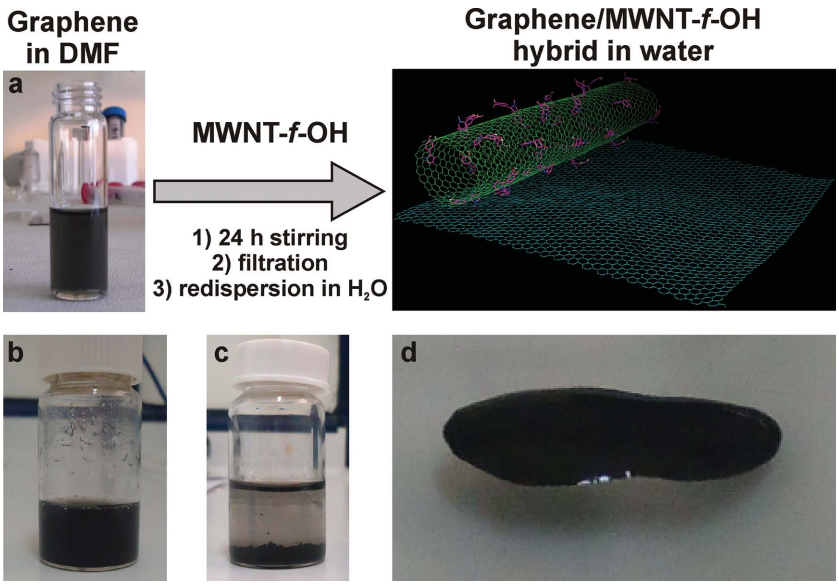

Figure 1. a) Scheme showing the formation of a graphene/MWNT-*f*-OH superstructure. b) Dispersion of the hybrid in water (15 mg mL^{-1}). c) Water dispersion without the addition of MWNT-*f*-OH; pristine graphene nanosheets were precipitated after the dispersion in DMF, centrifugation, and redispersion in water. d) Highly concentrated mixture of the hybrid in ethylene glycol.

compatibility with hydrophilic polymers and biomolecules, chemical inertness, and stability under normal conditions. Currently, the most attractive potential applications of carbon nanoallotropes include, for example, flexible transparent conductive films or low cost conductive inks for inkjet printing electronic circuits, radio-frequency (RF) antennas, energy storage, displays, photovoltaics, health diagnostic, spintronic nanodevices, and nanoelectromechanical systems.[10–20]

Since pristine graphene is extremely hydrophobic, its dispersion in water is totally prohibited without the assistance of covalently attached hydrophilic groups or through van der Walls adsorbed surfactants. For example, hydrophilic groups can be covalently attached onto graphene, dramatically altering its character from hydrophobic to hydrophilic. However, this modification also substantially modifies the conductivity and other basic properties of graphene by disrupting the extended aromatic system.[21] By using surfactants, ionic liquids, or hydrophilic polymers, stable dispersions of graphene in water have been produced.[9,22–25] In these cases, the derived graphene nanostructures retain their valuable optoelectronic and mechanical properties because the aromatic character is not affected by the noncovalent interactions. However, the main drawback of this approach lies in the unavoidable partial or complete covering of the graphene nanosheets by surfactant molecules, which frequently cause difficulties in applications, e.g., the electrical conductivity of a thin film made from surfactant stabilized graphene nanosheets is limited due to poor interconnection between the graphene nanosheets. Analogous difficulties are expected as a result of restriction of the active surface area of such graphene composites.

In this paper, we present an effective procedure for dispersion of a significant amount of pristine graphene nanosheets in water without the assistance of surfactants or polymers. The role of the stabilizer is provided by dihydroxyphenyl functionalized carbon nanotubes. The graphene/carbon nanotube hybrid was found to be highly dispersible in water and other polar organic solvents, such as ethanol, isopropanol, *N*,*N*-dimethylformamide (DMF), ethylene glycol (EG), and their mixtures. The superstructure exhibits not only the record dispersibility in water but also the excellent electrical conductivity enabling its applicability in conductive ink technologies or highly conductive polymers.

2. Results and Discussion

The hydroxyphenyl-functionalized multiwalled carbon nanotubes (MWNT-*f*-OH) were produced by 1,2-dipolar cycloaddition as described in our previous report.[26] The procedure for the preparation of water dispersion of graphene/MWNT-*f*-OH is described schematically in **Figure 1**a.

Briefly, a dispersion of graphene nanosheets in DMF (≈0.35 mg mL^{-1}) was prepared by exfoliating natural graphite under sonication. Specifically, a mixture of 70 mg graphite in 70 mL DMF was sonicated for 6 h and then the upper 60 mL of the suspension was isolated after an overnight precipitation of the unexfoliated graphite. The as-prepared dispersion contained mostly few layer graphene nanosheets and single graphene monolayers.[21,26,27] An amount of MWNT-*f*-OH (1 mg) was then mixed with 40 mL of the graphene/DMF dispersion by stirring, followed by removal of the solvent by filtration through a PTFE membrane or centrifugation (15 000 rpm for 10 min). The solid residue was then easily redispersed in 1 mL of water, affording a highly concentrated dispersion that contained about 15 mg mL^{-1} of the hybrid nanomaterial, which corresponds to 14 mg mL^{-1} graphene and 1 mg mL^{-1} MWNT-*f*-OH (Figure 1b).

A blank experiment was also performed whereby a graphene suspension in DMF (0.35 mg mL^{-1}) was filtered and redispersed from the filter into water yielded large aggregates that were totally not dispersible in water and precipitated rapidly (Figure 1c). Evidently, the hydrophilic groups of MWNT-*f*-OH permitted the hybrid nanostructure to form stable dispersions in water. A suspension of 15 mg mL^{-1} of the hybrid in water was stable for at least one week. It is worth mentioning that even highly concentrated suspensions of 25–30 mg mL^{-1} were also produced as a dark black liquid with a high viscosity. Using a H_2O/EG mixture (4:1), 30 mg of the hybrid was successfully dispersed in 1 mL of solvent, affording one of the most concentrated stable suspensions of graphene reported to date. The lifetime of such highly concentrated suspensions could be extended by simple daily agitation. Finally, 20 mg of the hybrid mixed homogenously with 200 µL of EG yielding a highly viscous black liquid that could be used as conductive paste (Figure 1d). We would like to emphasize that graphene/MWNT-*f*-OH hybrid is readily dispersible also in other polar solvents including ethanol, isopropanol, ethylene glycol, and

N,N-dimethylformamide (Figure S1, Supporting Information). The driving force for this interaction involves remarkable hydrogen bond between the hydroxy groups of the hybrid and solvents. Furthermore, the high viscosity of ethylene glycol improves the stability of the dispersion decelerating the reaggregation of the graphene sheets.

Solid-state atomic force microscopy (AFM) images and cross-section analyses of the prepared superstructures are shown in **Figure 2**a–c evidencing the few-layered character of graphene (up to 3 nm) interacting with carbon nanotubes (with diameters in tens of nm). Clearly, the nanotubes modify both edges and basal plane of graphene nanosheets. Importantly, the high degree of interaction is observable even during in situ liquid mode AFM measurements in water (see Figure 2d) where several nanotubes are entrapped among graphene nanosheets.

The Raman spectrum of the hybrid product exhibited the characteristic D and G bands at 1353 and 1584 cm^{-1}, respectively, with $I_D/I_G = 0.4$ and a single symmetrical G' band at 2708 cm^{-1} almost equal in height to the G band (**Figure 3**a). The I_D/I_G ratio of the composite was enhanced compared to that of pure pristine graphene ($I_D/I_G = 0.2$), most likely due to the contribution of the functionalized MWNT-*f*-OH (with $I_D/I_G = 0.6$ due to the covalent functionalization and character of MWNT) to the Raman spectrum of the hybrid. The intense symmetrical G′ band indicated the existence of single and few-layer graphene nanosheets in accordance with AFM data.

C1*s* core level X-ray photoelectron spectroscopy (XPS) spectrum of the graphene/MWNT-*f*-OH hybrid is shown in Figure 3b. After deconvolution with mixed Gaussian–Lorentzian functions, the C1*s* spectrum consists of six components. The dominant peak at a binding energy of 284.6 eV is attributed to the C–C and C–H bonds from graphene and the functionalized MWNT-*f*-OH. The second peak at 285.7 eV is correlated with the C–O (hydroxyl) and C–N bonds from the

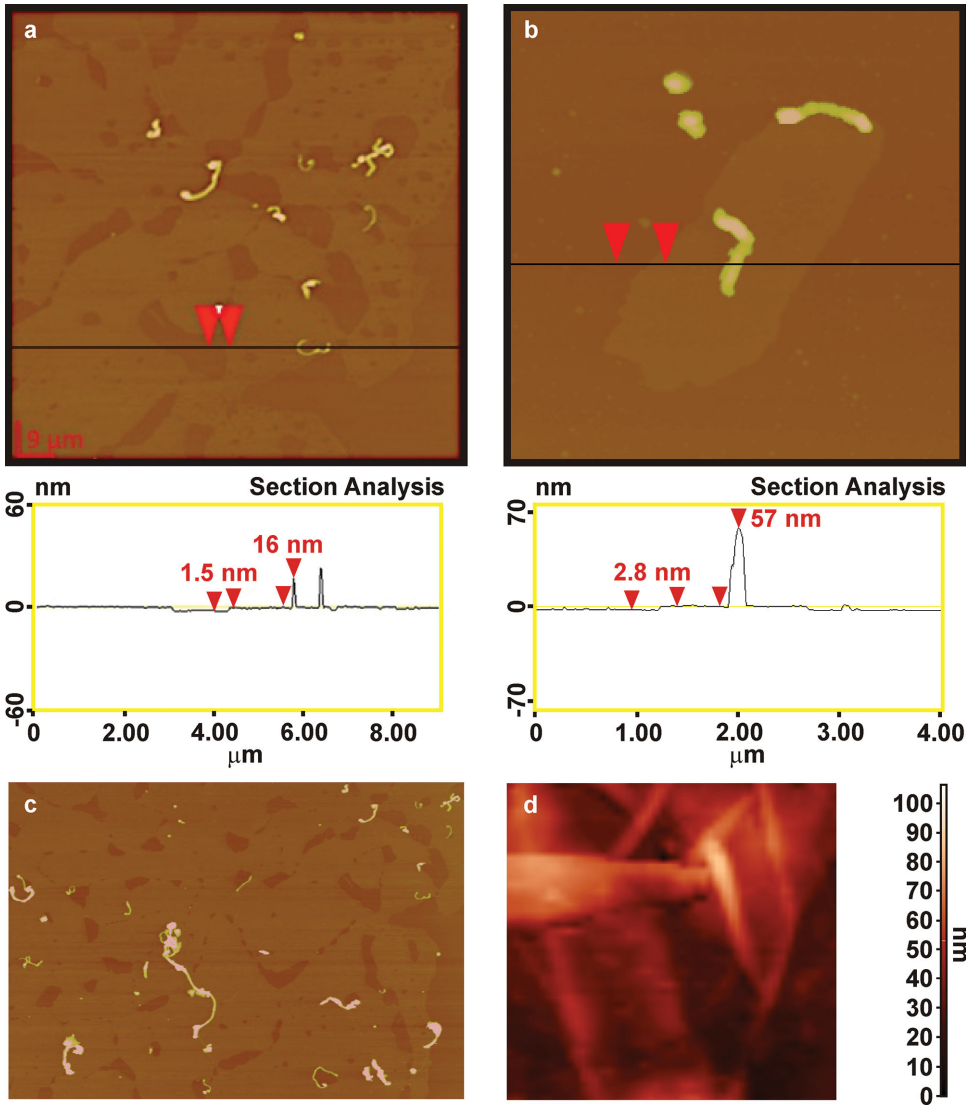

Figure 2. a–c) AFM images of graphene/MWNT-*f*-OH hybrid including height profiles demonstrating few layered graphene covered with carbon nanotubes with heights ranging from 15 to 60 nm; d) Liquid-mode in situ AFM image of graphene/MWNT-*f*-OH showing a high affinity of MWNT-*f*-OH to graphene in water.

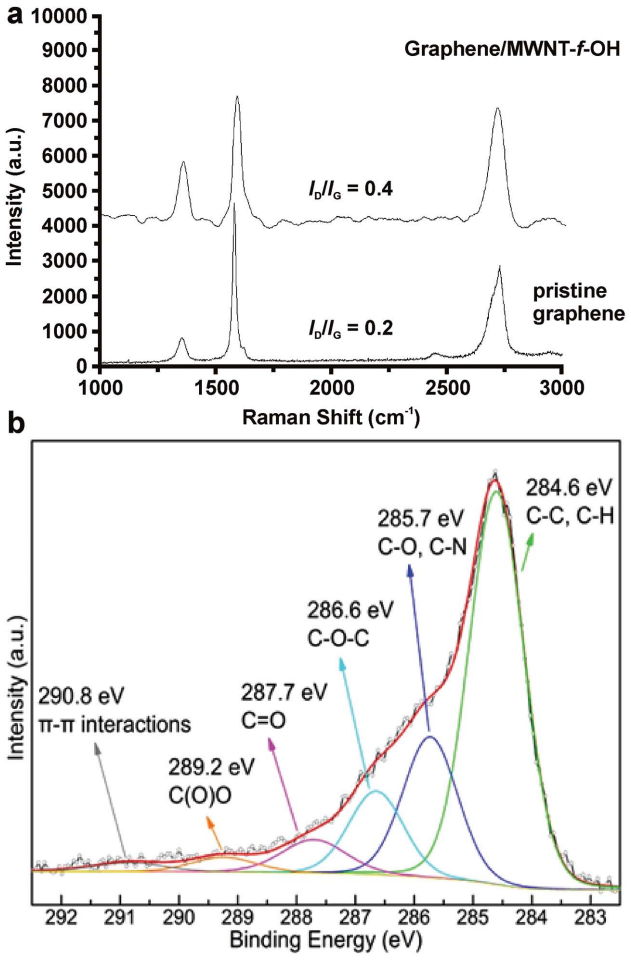

Figure 3. a) Raman spectra of graphene/MWNT-*f*-OH and pristine graphene and b) C1*s* core level X-ray photoemission spectrum of graphene/MWNT-*f*-OH hybrid.

functionalized MWNT-*f*-OH, whereas the C–O–C epoxide/ether groups correspond to the third component at 286.6 eV. The peak centered at 287.7 eV originates from carbonyl functional groups (C=O), while the contribution recorded at 289.2 eV is ascribed to the carboxyl groups (O–C=O).[28] Nevertheless, there is an additional peak at a higher binding energy of 290.8 eV that cannot be associated with any bond and arises from π–π interactions.[29] The presence of this shake-up satellite peak from π–π transitions between graphene and MWNT-*f*-OH points out that the functionalized MWNT-*f*-OH are attached through van der Walls interactions onto graphene surfaces due to the aromatic character of both components.[30]

To uncover the reasons of a high dispersibility of graphene/MWNT-f-OH hybrid in water, complex microscopic analyses (transmission electron microscopy (TEM)/high-resolution transmissionelectron microscopy (HRTEM), scanning electron microscopy (SEM), and AFM) and molecular dynamic simulations were performed. The microscopic images of the graphene/MWNT-*f*-OH hybrid (**Figure 4**) clearly showed different types of interaction between graphene nanoplatelets and carbon nanotubes. Specifically, MWNT-*f*-OH overlie the graphene nanoplatelets (Figure 4a,b), are trapped between the graphene layers, resulting in a partial change of their morphology (Figure 4c–f), or interact preferentially at the edges of graphene (Figure 4g,h). Moreover, the microscopic data revealed that almost all the carbon nanotubes interacted with graphene since there are no free carbon nanotubes out of the sheets; this is a strong indication that this interaction exists also in the liquid phase.

For theoretical modeling of the interaction between graphene and MWNT-*f*-OH, we used molecular dynamic simulations. Taking into account that the MWNT-*f*-OHs have diameters in tens of nanometers, we may assume that the contact area between graphene and MWNT-*f*-OH is rather flat. Therefore, we simulated the graphene–MWNT-*f*-OH system as an interaction between circumcoronene (C_{54}, representing graphene) and circumcoronene bearing one functional group (C_{54}-*f*-OH, representing MWNT-*f*-OH). **Figure 5** shows the potential of mean force (PMF) between two C_{54} sheets and between C_{54} and C_{54}-*f*-OH. The PMF clearly manifests that affinity of C_{54} to C_{54}-*f*-OH is approximately four times smaller than that between two C_{54} sheets. On the other hand, the formation of an assembly between graphene and MWNT-f-OH is kinetically preferred, as there are no significant barriers on the association curve of C_{54} and C_{54}-*f*-OH. Despite of the fact that the aggregation of graphene sheets is thermodynamically favored process, it seems that it is kinetically blocked by formation of graphene/MWNT-*f*-OH hybrid.

No doubt that the water dispersibility opens the doors for new applications of graphene and its hybrid with MWNT-*f*-OH. Thus, we have studied the application potential of highly concentrated graphene/MWNT-*f*-OH hybrid dispersion in water for a conductive ink (see Figure S2, Supporting Information). Pristine graphene nanosheets have been shown to have much more favorable electrical properties than *r*GO. In addition, the absence of surfactant molecules, organic additives, or polymers in the water phase and between the graphene nanosheets caused that the interconnection of graphene nanosheets was less electrically resistive. CNTs, graphene oxide, graphene, and their hybrids with conductive polymers have been used as carbon based inks usually in low concentrations due to their hydrophobic nature, limiting the stability of the system as described extensively in a recent review on solution processing approaches for material ink formulations for organic electronics.[18] To compare conductive properties of our system, spots of the graphene/MWNT-*f*-OH hybrid (≈300 µg dispersed in circular spots with a diameter of ≈0.8 cm and a thickness of about 2.86 µm) deposited on paper by drop casting of the as-prepared water dispersion (15 µg µL^{-1}) showed a minimum sheet resistance of $R_s \approx 25\ \Omega\ sq^{-1}$. This is reflected in the electrical conductivity of 14 000 S m^{-1}, which is among the highest values reported in the literature for a material synthesized from natural graphite and without annealing or other complex procedures.[27] One of the most remarkable advantages of the hybrid is that the electrical conductivity was not altered when the "graphitic paper" was highly curved (**Figure 6**a).

Similar sized spots of more concentrated hybrid suspensions (e.g., 20 µL of a suspension of 30 µg µL^{-1}) showed even a much lower sheet resistance ($R_s \approx 5\ \Omega\ sq^{-1}$ or a maximum conductivity of 28 000 S m^{-1}). However, the stability of the spots in paper, in this case, was limited (forming a graphitic flake that was easily

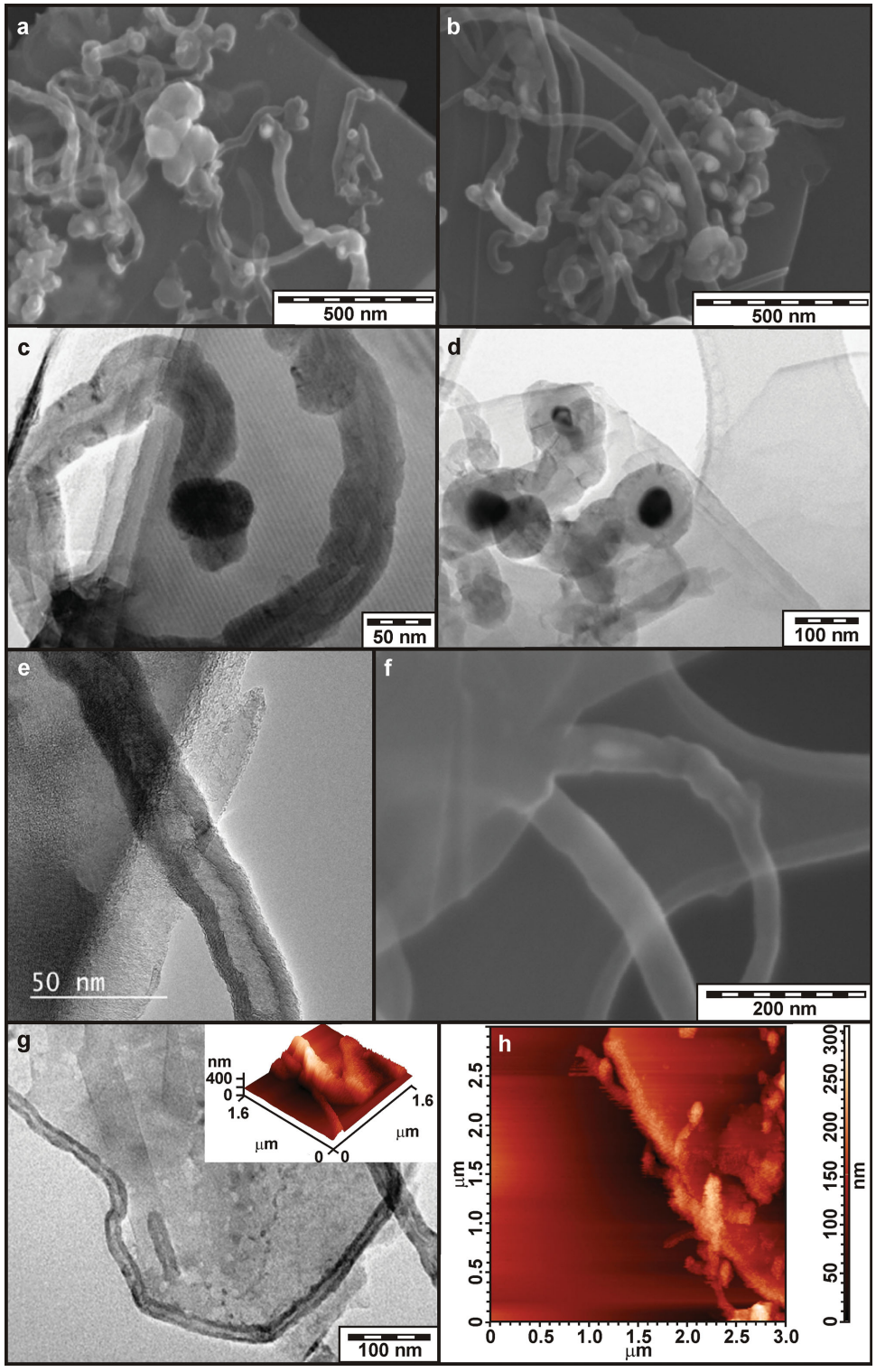

Figure 4. a,b) SEM images of the hybrid showing MWNT-*f*-OH overlying graphene nanoplatelets; c–f) SEM and TEM and HRTEM images of the hybrid showing MWNT-*f*-OH trapped between graphene layers; g,h) TEM and AFM images demonstrating the interaction at the edges of graphene.

removed from the paper). The graphene/MWNT-*f*-OH hybrid suspension (30 mg mL^{-1} in H_2O/EG, 4:1) was further tested as a potential ink for inkjet printing techniques. A printed line made after 20 passes was clearly conductive (Figure 6b). Finally, the hydrophilic character of the hybrid facilitates its fine dispersion in water-soluble polymers such as polyvinyl alcohol (PVA) forming highly conductive composites (Figure 6c). The PVA/graphene/MWNT-*f*-OH composite prepared in such a way,

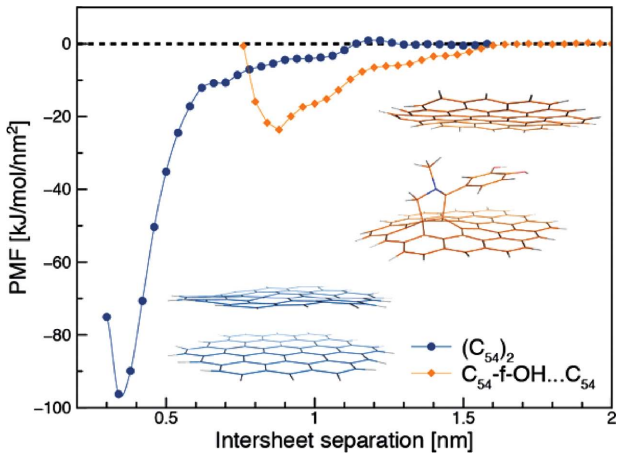

Figure 5. The PMF for interaction of graphene–graphene (blue) and graphene–nanotube (orange) models in water.

with a hybrid weight ratio of 20%, showed a conductivity of 285 S m^{-1} (or a sheet resistance of $R_s \approx 1300\ \Omega\ sq^{-1}$, whereas the film thickness was estimated to 2.7 μm) which is one of the highest values reported for graphene based systems in the literature.[31]

3. Conclusion

We describe an easy, scalable, and surfactant free route for effective dispersion of pristine graphene in water through the self-assembly with OH-functionalized hydrophilic nanotubes. The nanotube assisted dispersibility of graphene in water is kinetically driven with several modes of interaction involving the nanotube trapping between the graphene sheets or modification of graphene edges. This 2D/1D carbon superstructure creates the stable water dispersion at concentrations up to 15 mg mL^{-1} and is readily dispersible also in other polar solvents. Moreover, it exhibits excellent electrical conductivity thus providing the huge application potential in inkjet printing technologies or as highly conductive polymers.

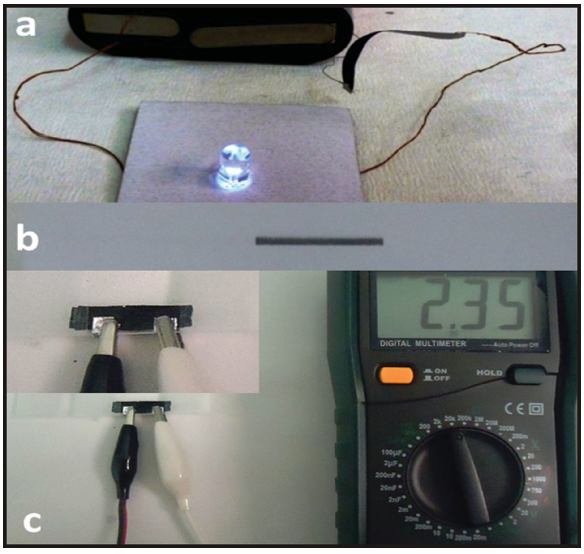

Figure 6. a) Simple electrical circuit representing the electrical conductivity of a curved paper painted with the graphene/MWNT-*f*-OH hybrid. b) A printed line of graphene hybrid ink on a paper ribbon. c) Conductive composite film made by graphene/MWNT-*f*-OH hybrid in PVA (20% w/w).

4. Experimental Section

Raman spectroscopy was performed on a Micro-Raman system RM 1000 RENISHAW using a laser excitation line at 532 nm (Nd-YAG - neodymium-doped yttrium aluminum garnet-type laser). A power of 0.5–1 mW was used with a 1 μm focus spot in order to avoid photodecomposition of the samples.

TEM images were obtained using a JEM2010 microscope operated at 200 kV with a point-to-point resolution of 1.9 Å. Before the measurements, the samples were dispersed in ethanol and the suspension was treated in ultrasound for 10 min. A drop of very dilute suspension was placed on a carbon-coated grid and allowed to dry by evaporation at ambient temperature. HRTEM images were obtained by HRTEM TITAN 60-300 with X-FEG type emission gun, operating at 80 kV. This microscope is equipped with Cs image corrector and a STEM high-angle annular dark-field detector (HAADF). The point resolution is 0.06 nm in TEM mode. The elemental mappings were obtained by STEM-EDS (scanning transmission electron microscopy–energy dispersive X-ray spectroscopy) technique with acquisition time 20 min. For HRTEM analyses, the powder samples were dispersed in ethanol and ultrasonicated for 5 min. One drop of this solution was placed on a copper grid with holey carbon film. The sample was dried at room temperature. SEM imaging was performed using an EVO MA10 (ZEISS). AFM images were obtained in tapping mode with a 3D Multimode Nanoscope, using Tap-300G silicon cantilevers with a tip radius of <10 nm and a force constant of ≈20–75 N m^{-1}. Samples were deposited onto silicon wafers (P/Bor, single side polished) from aqueous solutions by drop casting. The hybrid sample was also measured in the semicontact mode on an NTegra Aura atomic force microscope with an NT-MDT CSG10 cantilever under liquid conditions in deionized water and at room temperature. The solvent for the sample was water, which was used to deposit the sample on freshly cleaved highly ordered pyrolytic graphite (HOPG) and let to dry for 30 min so that hybrids could attach to the substrate at 40 °C. The liquid measurement was then performed in an open liquid cell after additional deionized water was added and the system reached stable conditions.

XPS measurements were performed under ultrahigh vacuum conditions with a base pressure of 5×10^{-10} mbar in a SPECS GmbH instrument equipped with a monochromatic MgKα source ($h\nu$ = 1253.6 eV) and a Phoibos-100 hemispherical analyzer. A minute quantity of the graphene/MWNT-*f*-OH suspension in H_2O was drop cast on silicon wafer and left to dry in air before transfer to ultrahigh vacuum. The energy resolution was set to 0.3 eV and the photoelectron take-off angle was 45° with respect to the surface normal. Recorded spectra were the average of three scans with energy step set to 0.05 eV and dwell time 1 s. All binding energies were referenced to the C1*s* core level at 284.6 eV. Spectral analysis included a Shirley background subtraction and peak deconvolution employing mixed Gaussian–Lorentzian functions, in a least squares curve-fitting program (WinSpec) developed at the Laboratoire Interdisciplinaire de Spectroscopie Electronique, University of Namur, Belgium.

Electrical measurements were performed using the four-probe technique, an AFX DC 9660SB power supply, and Keithley 2000 multimeter. The printed line was made using an HP Deskjet D2400 printer.

Molecular dynamics (MD) simulations were carried out using Gromacs 5.0 software package.[32] After equilibration in the *NPT* ensemble (N = 6387 (C_{54}), 6392 (C_{54}-*f*-OH), P = 1.0 bar, T = 300 K), production runs were performed in the *NVT* ensemble (V = 61.6 nm^3, T = 300 K). All atom optimized-potentials-for-liquid-simulations (OPLS)

force field parameters[33] were used for atoms in functional group and the SPC/E model was used for water.[34] The intermolecular interactions of graphene atoms with surrounding molecules were treated by the Lennard-Jones potential using form suggested by Chang and Steele,[35] which provides interaction enthalpies of organic molecules to graphene with a good agreement with the experiment.[36] The integration step for all simulations was 2 fs and the interval for data collection was set to 0.5 ps. The cutoff distance for the direct electrostatics and van der Waals potential was set to 1 nm. The particle mesh Ewald method was used to calculate the indirect electrostatic potential beyond the cutoff distance. Bonds to hydrogen atoms were constrained during the MD simulations using the noniterative linear-constraint-solver (LINCS) algorithm. The PMF of interaction between C_{54} and C_{54}, and C_{54} and C_{54}-*f*-OH was calculated using constrained MD simulations in extended-simple-point-charge (SPC/E) explicit water solvent. The 1.2 nm long reaction coordinate was divided into 32 equally spaced windows with the step size of 0.04 nm. Each window was equilibrated for 2 ns and 10 ns were used for data collection. The total force acting on one fixed inner carbon atom of a C_{54} was collected every 0.5 ps, while all carbons of the second sheet (C_{54} or C_{54}-*f*-OH) were fixed. The average force in each window was integrated using the trapezoidal method.

Supporting Information

Supporting Information is available from the Wiley Online Library or from the author.

Acknowledgements

The authors gratefully acknowledge the support by the project LO1305 of the Ministry of Education, Youth and Sports of the Czech Republic, the Operational Program Education for Competitiveness: European Social Fund (Project No. CZ.1.07/2.3.00/20.0017) of the Ministry of Education, Youth and Sports of the Czech Republic, and the Grant Agency of the Czech Republic (Grant No. P208/12/G016). This work was also cofinanced by the European Union (European Social Fund—ESF) and Greek national funds through the Operational Program "Education and Lifelong Learning" of the National Strategic Reference Framework (NSRF)—Research Funding Program: THALES—Investing in Knowledge Society through the European Social Fund. The authors thank Dr. K. Čépe and Dr. J. P. Froning for the microscopic observations and Dr. J. Tuček and Dr. J. A. Perman for technical assistance.

Received: October 29, 2014
Revised: December 8, 2014
Published online: January 14, 2015

[1] K. S. Novoselov, V. I. Fal'ko, L. Colombo, P. R. Gellert, M. G. Schwab, K. Kim, *Nature* **2012**, *490*, 192.
[2] K. S. Novoselov, A. K. Geim, S. V. Morozov, D. Jiang, Y. Zhang, S. V. Dubonos, I. V. Grigorieva, A. A. Firsov, *Science* **2004**, *306*, 666.
[3] S. Park, R. S. Ruoff, *Nat. Nanotechnol.* **2009**, *4*, 217.
[4] Y. Hernandez, V. Nicolosi, M. Lotya, F. M. Blighe, Z. Y. Sun, S. De, I. T. McGovern, B. Holland, M. Byrne, Y. K. Gun'ko, J. J. Boland, P. Niraj, G. Duesberg, S. Krishnamurthy, R. Goodhue, J. Hutchison, V. Scardaci, A. C. Ferrari, J. N. Coleman, *Nat. Nanotechnol.* **2008**, *3*, 563.
[5] C. E. Hamilton, J. R. Lomeda, Z. Sun, J. M. Tour, A. R. Barron, *Nano Lett.* **2009**, *9*, 3460.
[6] A. B. Bourlinos, V. Georgakilas, R. Zboril, T. A. Steriotis, A. K. Stubos, *Small* **2009**, *5*, 1841.
[7] P. Blake, P. D. Brimicombe, R. R. Nair, T. J. Booth, D. Jiang, F. Schedin, L. A. Ponomarenko, S. V. Morozov, H. F. Gleeson, E. W. Hill, A. K. Geim, K. S. Novoselov, *Nano Lett.* **2008**, *8*, 1704.
[8] V. Georgakilas, A. Kouloumpis, D. Gournis, A. Bourlinos, C. Trapalis, R. Zboril, *Chem. Eur. J.* **2013**, *19*, 12884.
[9] A. Ciesielski, P. Samori, *Chem. Soc. Rev.* **2014**, *43*, 381.
[10] X. Wang, L. Zhi, K. Mullen, *Nano Lett.* **2008**, *8*, 323.
[11] L. G. De Arco, Y. Zhang, C. W. Schlenker, K. Ryu, M. E. Thompson, C. Zhou, *ACS Nano* **2010**, *4*, 2865.
[12] J. Wu, M. Agrawal, H. A. Becerril, Z. Bao, Z. Liu, Y. Chen, P. Peumans, *ACS Nano* **2010**, *4*, 43.
[13] T. A. Elwi, H. M. Al-Rizzo, D. G. Rucker, E. Dervishi, Z. R. Li, A. S. Biris, *Nanotechnology* **2010**, *21*, 045301.
[14] X. Han, Y. Chen, H. Zhu, C. Preston, J. Wan, Z. Fang, L. Hu, *Nanotechnology* **2013**, *24*, 205304.
[15] E. B. Secor, P. L. Prabhumirashi, K. Puntambekar, M. L. Geier, M. C. Hersam, *J. Phys. Chem. Lett.* **2013**, *4*, 1347.
[16] F. Torrisi, T. Hasan, W. Wu, Z. Sun, A. Lombardo, T. S. Kulmala, G. W. Hsieh, S. Jung, F. Bonaccorso, P. J. Paul, D. Chu, A. C. Ferrari, *ACS Nano* **2012**, *6*, 2992.
[17] J. Tucek, K. C. Kemp, K. S. Kim, R. Zboril, *ACS Nano* **2014**, *8*, 7571.
[18] Y. Aleevaa, B. Pignataroa, *J. Mater. Chem. C* **2014**, *2*, 6436.
[19] A. Candini, S. Klyatskaya, M. Ruben, W. Wernsdorfer, M. Affronte, *Nano Lett.* **2011**, *11*, 2634.
[20] M. Ganzhorn, S. Klyatskaya, M. Ruben, W. Wernsdorfer, *Nat. Nanotechnol.* **2013**, *8*, 165.
[21] V. Georgakilas, M. Otyepka, A. B. Bourlinos, V. Chandra, N. Kim, K. C. Kemp, P. Hobza, R. Zboril, K. S. Kim, *Chem. Rev.* **2012**, *112*, 6156.
[22] Y. T. Liang, M. C. Hersam, *J. Am. Chem. Soc.* **2010**, *132*, 17661.
[23] T. Kim, H. W. Lee, J. E. Kim, K. S. Suh, *ACS Nano* **2010**, *4*, 1612.
[24] Y. Lin, J. Jin, O. Kusmartsev, M. Song, *J. Phys. Chem. C* **2013**, *117*, 17237.
[25] M. Lotya, P. J. King, U. Khan, S. De, J. N. Coleman, *ACS Nano* **2010**, *4*, 3155.
[26] V. Georgakilas, A. Bourlinos, D. Gournis, T. Tsoufis, C. Trapalis, A. Mateo-Alonso, M. Prato, *J. Am. Chem. Soc.* **2008**, *130*, 8733.
[27] N. Behabtu, J. R. Lomeda, M. J. Green, A. L. Higginbotham, A. Sinitskii, D. V. Kosynkin, D. Tsentalovich, A. N. G. Parra-Vasquez, J. Schmidt, E. Kesselman, Y. Cohen, Y. Talmon, J. M. Tour, M. Pasquali, *Nat. Nanotechnol.* **2010**, *5*, 406.
[28] R. Y. N. Gengler, D. S. Badali, D. Zhang, K. Dimos, K. Spyrou, D. Gournis, R. J. D. Miller, *Nat. Commun.* **2013**, *4*, 2560.
[29] S. Biniak, G. Szymański, J. Siedlewski, A. Świątkowski, *Carbon* **1997**, *35*, 1799.
[30] K. Spyrou, M. Calvaresi, E. K. Diamanti, T. Tsoufis, D. Gournis, P. Rudolf, F. Zerbetto, *Adv. Funct. Mater.* **2014**, DOI: 10.1002/adfm.201402622.
[31] C. Wu, X. Huang, G. Wang, L. Lv, G. Chen, G. Li, P. Jiang, *Adv. Funct. Mater.* **2013**, *23*, 506.
[32] D. Van der Spoel, E. Lindahl, B. Hess, G. Groenhof, A. E. Mark, H. J. C. Berendsen, *J. Comput. Chem.* **2005**, *26*, 1701.
[33] W. L. Jorgensen, J. Tirado-Rives, *Proc. Natl. Acad. Sci. U.S.A.* **2005**, *102*, 6665.
[34] H. J. C. Berendsen, J. R. Grigera, T. P. Straatsma, *J. Phys. Chem.* **1987**, *91*, 6269.
[35] A. Cheng, W. A. Steele, *J. Chem. Phys.* **1990**, *92*, 3858.
[36] P. Lazar, F. Karlický, P. Jurečka, M. Kocman, E. Otyepková, K. Šafářová, M. Otyepka, *J. Am. Chem. Soc.* **2013**, *135*, 6372.